

Telecommunications-band heralded single photons from a silicon nanophotonic chip

Marcelo Davanço,^{1,2} Jun Rong Ong,³ Andrea Bahgat Shehata,⁴
Alberto Tosi,⁴ Imad Agha,^{1,2} Solomon Assefa,⁵ Fengnian Xia,⁵
William M.J. Green,⁵ Shayan Mookherjea,^{3,*} and Kartik Srinivasan^{1,†}

¹*Center for Nanoscale Science and Technology,
National Institute of Standards and Technology, Gaithersburg, MD 20899, USA*

²*Maryland NanoCenter, University of Maryland, College Park, MD 20742, USA*

³*University of California, San Diego,
Mail Code 0407, La Jolla, California 92093*

⁴*Politecnico di Milano, Dipartimento di Elettronica e Informazione,
Piazza Leonardo da Vinci 32, 20133 Milano, Italy*

⁵*IBM Thomas J. Watson Research Center,
Yorktown Heights, New York 10598*

(Dated: April 16, 2012)

Abstract

We demonstrate room temperature heralded single photon generation in a CMOS-compatible silicon nanophotonic device. The strong modal confinement and slow group velocity provided by a coupled resonator optical waveguide produced a large four-wave-mixing nonlinearity coefficient $\gamma_{\text{eff}} \approx 4100 \text{ W}^{-1}\text{m}^{-1}$ at telecommunications wavelengths. Spontaneous four-wave-mixing using a degenerate pump beam at 1549.6 nm created photon pairs at 1529.5 nm and 1570.5 nm with a coincidence-to-accidental ratio exceeding 20. A photon correlation measurement of the signal (1529.5 nm) photons heralded by the detection of the idler (1570.5 nm) photons showed anti-bunching with $g^{(2)}(0) = 0.19 \pm 0.03$. The demonstration of a single photon source within a silicon platform holds promise for future integrated quantum photonic circuits.

* smookherjea@ucsd.edu

† kartik.srinivasan@nist.gov

Quantum photonics on a chip [1] promises the combination of high-performance, device integration, and scalability needed for many quantum-enabled technologies in information processing, communications, and metrology. This has motivated much effort in developing chip-based quantum components for the generation, manipulation, and detection of quantum states. Recently, waveguide quantum circuits [2] have demonstrated quantum interference and entanglement manipulation using off-chip light sources [3, 4]. On-chip single photon sources based on the radiative decay of a single quantum emitter such as a quantum dot [5] have also been developed, but typically operate at wavelengths outside the 1550 nm telecommunications window, require cryogenic temperatures, and use III-V semiconductors. Quantum photonic devices in silicon are of particular interest, given its dominant role as a platform supporting systems of scalable complexity, such as microelectronics, micromechanics, and microphotonics. Here, we demonstrate room temperature single photon generation from a CMOS-compatible silicon nanophotonic device operating in the telecommunications-band. This device complements recent demonstrations of quantum interference [6] and single photon detection [7] in silicon nanophotonics, and represents a step towards achieving highly-functional silicon-based integrated quantum photonic systems.

There are two dominant approaches to single photon generation at optical wavelengths. The first is through radiative decay of a single quantum emitter that is “triggered” by excitation pulses. The second, which we use here, is through spontaneous photon pair production, in which the detection of one photon of the pair provides the time stamp by which the remaining (“heralded”) single photon is identified. Both approaches for single photon generation were first demonstrated in bulk optical systems decades ago [8–10]. Since then, chip-based triggered single photon sources, typically based on cryogenically-cooled systems such as epitaxially-grown quantum dots [5], have been widely studied. In contrast, heralded single photon generation, which is usually based on nonlinear processes achievable in a broader class of materials and at room temperature, has primarily been studied in larger systems such as bulk crystals [11, 12], quasi-phase-matched waveguides [13–15], and optical fibers [16–19]. Recently, however, researchers have begun exploring four-wave-mixing (FWM) and photon pair production in CMOS-compatible silicon nanophotonic devices [20–23], which support a strong third-order optical nonlinearity over a wide range of infrared wavelengths which can be chosen by the designer. Here, we advance previous work and demonstrate not only photon pair production, but also explicitly show heralded single photon

generation in a silicon nanophotonic device near the 1.55 μm telecommunications band. We make use of recently developed high trigger rate telecommunications-band single photon counters [24] to perform the three detector experiment needed for this demonstration.

Since silicon lacks a second-order optical nonlinearity, photon pair production uses the third-order (ultrafast Kerr) nonlinearity, typically in the degenerate four-wave-mixing configuration where a single pump beam at frequency ω_p generates photons at signal (ω_s) and idler (ω_i) frequencies, with energy conservation requiring $2\omega_p = \omega_s + \omega_i$ and momentum conservation (phase-matching) being a requirement for appreciable pair production. Silicon nanophotonic waveguides have an effective nonlinearity coefficient $\gamma_{\text{eff}} \approx 100 - 200 \text{ W}^{-1}\text{m}^{-1}$ that is four orders of magnitude larger than that of highly nonlinear optical fiber [20, 21]. Also, spontaneous Raman scattering, a broadband noise source in optical fiber based photon sources which requires them to be cryogenically-cooled [25], is generally less important in silicon, where it is narrowband and more easily avoided either by spectral filtering after the silicon waveguide structure, or even more advantageously by inhibiting propagation at the Raman-shifted wavelength (as in the device used here). Silicon waveguides, however, exhibit two-photon absorption (TPA) and free-carrier absorption (FCA) at high pump powers, and should be made as compact as possible since on-chip footprint is a highly valuable resource in CMOS silicon technology.

Our device geometry is a silicon coupled-resonator optical-waveguide (CROW) as shown in Fig. 1(a). The CROW consists of $N = 35$ directly-coupled microring resonators (loss = 0.21 dB/ring), such that each eigenmode is a collective resonance of all N resonators. Light is transmitted through the CROW in a disorder-tolerant slow light regime, with slowing factor $S = n_{\text{g,CROW}}/n_{\text{g,WG}}$ between 5 and 12, depending on the wavelength ($n_{\text{g,CROW}}$ is the group index of the CROW; $n_{\text{g,WG}}$ is the group index of a conventional Si waveguide). As γ_{eff} is enhanced by a factor S^2 , the CROW achieves higher levels of conversion within the limited footprint available on a chip. Indeed, in ref. 26, we have shown classical FWM with $\gamma_{\text{eff}} \approx 4100 \text{ W}^{-1}\text{m}^{-1}$, representing +16 dB enhanced conversion compared to a conventional nanophotonic waveguide, for $> 10 \text{ THz}$ (80 nm) separation between signal and idler; similar reports have been obtained in other CROW devices (both microrings [27] and coupled photonic crystal defect resonators [28]). Slow-light enhanced wavelength conversion of such widely-separated wavelengths, which span a significant fraction of the fiber-optic telecommunications window, is difficult to achieve in conventional

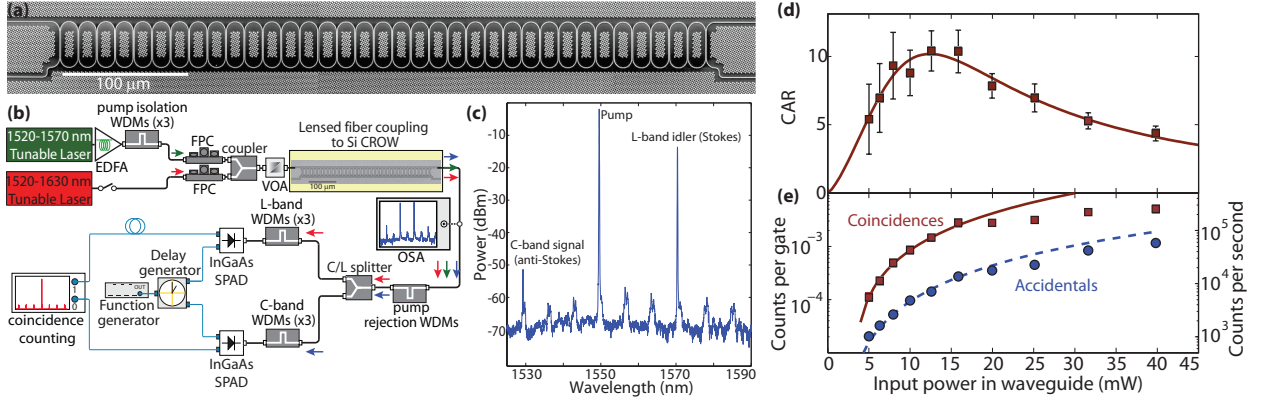


FIG. 1. Photon pair production in a silicon CROW. (a) Scanning electron microscope image of the 35-ring CROW used in this work. (b) Experimental setup used to measure correlated photon pairs generated by the CROW. The 1520 nm to 1630 nm tunable laser is used for stimulated FWM experiments to identify the signal and idler wavelengths, but is disconnected during SFWM/photon pair generation measurements. EDFA = erbium-doped fiber amplifier, WDM = wavelength division multiplexer, FPC = fiber polarization controller, VOA = variable optical attenuator, OSA = optical spectrum analyzer, SPAD = single photon avalanche diode. (c) FWM spectrum in which a 1549.6 nm pump amplifies a 1570.5 nm probe and generates a new field at 1529.5 nm. The spectral peaks in-between the pump and signal/idler fields are due to transmission of (unfiltered) EDFA spontaneous emission (ASE) through the CROW passbands. In photon pair measurements, this ASE is suppressed by > 150 dB by the pump isolation WDMs. (d) Coincidence-to-accidental ratio (CAR) as a function of power at the CROW input, for continuous wave pumping [26]. (e) Number of coincidences (red) and accidentals (blue) at the CROW output as a function of power at the CROW input. Results are plotted in units of (left y-axis) counts per gate and (right y-axis) counts per second [27].

photonic crystal waveguides because of the limited bandwidth of their slow-light regime compared to CROWs; ≈ 1.25 THz (10 nm) signal-idler separation was reported in ref. 23. This wide wavelength separation is of practical benefit in spectrally isolating the members of the photon pair from residual pump photons and each other.

We first show photon pair production from the Si CROW device, using the experimental setup depicted in Fig. 1(b). Time-correlated signal and idler photons are expected to be generated in multiple pairs of CROW transmission bands that are approximately equally

red- and blue-detuned from our amplified pump beam at 1549.6 nm, as demonstrated in previous classical FWM mixing experiments [26]. We choose a signal-idler pair at 1529.5 nm and 1570.5 nm, as shown in Fig. 1(c). Here, to show the classical FWM process, a strong pump at 1549.6 nm was combined with a probe field at 1570.5 nm, resulting in the addition of stimulated photons into the 1570.5 nm field and generation of a new field at 1529.5 nm. For spontaneous FWM (SFWM) experiments, the 1570.5 nm probe field was disconnected so that spontaneous photons are generated in the signal and idler bands. The 1549.6 nm pump was filtered to a 1.0 nm bandwidth through cascaded WDM and tunable filters, and light was coupled to and from the chip (loss = 5 dB per coupler) using tapered lensed fibers and polymeric overlaid waveguide couplers. Output light from the chip was filtered by a set of WDM pump-rejection filters (120 dB estimated pump rejection at 1550 nm \pm 3 nm) and then routed through cascaded C- and L- band WDM filters (estimated 150 dB pump isolation; 0.5 nm bandwidth) to spectrally separate and isolate the signal and idler photons, respectively. The signal (C-band) and idler (L-band) photons were detected by InGaAs/InP Single-Photon Avalanche Diodes (SPADs) gated electronically at 1 MHz (10 % detection efficiency, 20 ns gate width, and 10 μ s dead-time), and raw coincidences (C_{raw}) and accidentals (A_{raw}) were measured by a time-correlated single photon counting (TCSPC) system operating with 512 ps timing resolution, with typical measurement integration times between 1800 s and 5400 s. Coincidences due to dark counts (D) were measured separately for both integration times at each detector, and subtracted to yield $C = C_{\text{raw}} - A_{\text{raw}}$ and $A = A_{\text{raw}} - D$, with the coincidence-to-accidental ratio given as $\text{CAR} = C/A$ [29].

CAR under continuous wave (cw) excitation is shown in Fig. 1(d) as a function of the input power into the CROW. CAR initially increased and then rolled off at higher intensities, which is the anticipated behavior based on other studies [20–23], where at low powers CAR is thought to be limited by detector noise, while at higher powers, nonlinear loss and multiple pair generation are the limiting factors. Peak CAR was 10.4 ± 1.4 at an input power of 12 dBm, which was below the level for 1 dB excess nonlinear absorption in these CROWs [26]. In Fig. 1(e), we plot the coincidence and accidental rates at the output of the CROW [30]. At peak CAR, the coincidence rate is $\approx 1.5 \times 10^{-3}$ per detector gate; considering the cw pumping and the 1 MHz detector trigger rate and 20 ns gate width, this corresponds to a pair coincidence rate of ≈ 73 kHz. Figure 1(e) also shows quadratic fits (solid lines) to the six lowest power data points; the sub-quadratic dependence of C and A at higher pump powers

was most likely related to TPA/FCA effects. We compared the pair production performance of our CROW with a conventional single mode silicon wire waveguide (length of 2.63 cm, loss = 2.6 dB/cm, coupling loss = 5 dB per coupler) on the same chip. A peak CAR of 8.5 ± 1.0 was measured for this device, with a pair coincidence rate of 95 kHz. Thus, the CROW photon pair source moderately outperformed a conventional silicon waveguide whose physical footprint was 54 times longer.

We next consider heralded single photon generation from this device (Fig. 2(a)). Here, the detection of an L-band idler photon indicates (heralds) the presence of its twin, and a photon correlation measurement on these heralded photons confirms their single photon character [9, 10]. We pumped the CROW using a pulsed source, which was created by modulating and amplifying a tunable diode laser at 1549.6 nm to create 2.5 ns wide, 8 MHz repetition rate pulses. C-band signal and L-band idler photons were spectrally separated and isolated in the same way as above, but now the C-band signal photons were split by a 50/50 coupler, with each C-band path detected by an InGaAs/InP SPAD (20 % detection efficiency, 20 ns gate width, and no deadtime). The detectors in this Hanbury-Brown and Twiss photon correlation measurement setup (labeled SPAD B and SPAD C in Fig. 2(a)) were triggered by the detection of an L-band idler photon (the herald). The L-band photons were detected by a high-performance InGaAs/InP SPAD [24], labeled SPAD A in Fig. 2(a), which operates at 30 % detection efficiency, 10 ns gate width, and 10 μ s dead time and is triggered at 8 MHz by the electro-optic modulator driver. The normalized value of the photon correlation measurement on the C-band signal photons at zero time delay, $g^{(2)}(0)$, is given by $g^{(2)}(0) = \frac{N_{ABC}N_A}{N_{AB}N_{AC}}$ [31]. Triple coincidences N_{ABC} , corresponding to simultaneous events on all three detectors, were recorded over a 2.5 ns bin using the TCSPC. Double coincidences N_{AB} and N_{AC} , corresponding to simultaneous events on SPADs A and B or SPADs A and C, were given by the photon detection rates on SPAD B and SPAD C. The number of heralding photons N_A is determined by the detection rate on SPAD A, and a typical integration time of 1500 s was used for each measurement.

In Fig. 2(b), we plot the value of $g^{(2)}(0)$ as a function of average input power into the CROW. $g^{(2)}(0) < 0.5$ for all pump powers that we recorded, indicating that we indeed have a source that is antibunched and dominantly composed of single photons [32]. The minimum value we measured is $g^{(2)}(0) = 0.19 \pm 0.03$ at ≈ 1.7 mW of average power into the CROW. At lower power levels in our experiment, $g^{(2)}(0)$ may be limited by detector dark counts and

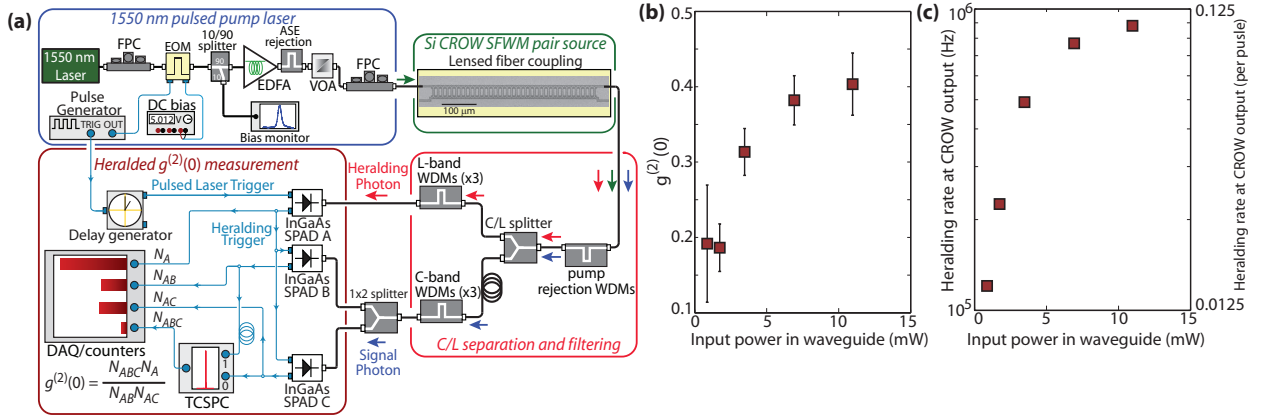


FIG. 2. Heralded single photon measurement. (a) Schematic of the experimental setup used to perform heralded single photon measurements. The Si CROW waveguide is pumped by a pulsed 1549.6 nm laser (2.5 ns pulses, 8 MHz repetition rate) generated by a modulated and amplified diode laser. Generated photon pairs are spectrally isolated and separated into the C-band (1529.5 nm) and L-band (1570.5 nm). Detection of an L-band photon by an InGaAs/InP SPAD is used to trigger a Hanbury-Brown and Twiss photon correlation measurement on the C-band photon. (b) Heralded $g^{(2)}(0)$ as a function of average power at the CROW input [30]. (c) Heralding rate at the CROW output as a function of average power at the CROW input. Results are plotted in units of (left y-axis) heralding photons per second and (right y-axis) heralding photons per pulse.

afterpulsing, while at higher power levels, the increase in $g^{(2)}(0)$ is likely due to the increased multi-photon probability as multiple photon pairs are generated in each optical pulse. The maximum power levels we can inject into the CROW were ultimately limited by the damage threshold of the input couplers. In Fig. 2(c), we plot the heralding rate (detection rate of L-band photons by SPAD A) at the CROW output. At the minimum value of $g^{(2)}(0)$, the heralding rate was ≈ 220 kHz (≈ 0.028 photons/pulse). As the input power to the CROW increases, the generation rate of heralding photons saturated near 1 MHz due to TPA/FCA effects in silicon. Under pulsed pumping (2.5 ns pulses, 8 MHz trigger rate) and at the input power corresponding to the minimum value of $g^{(2)}(0)$, $\text{CAR} \approx 15$ was measured without dark count subtraction. Subtraction of dark count coincidences (due to dark counts on both detectors as well dark counts on one detector and photon detection events on the other detector) yields $\text{CAR} = 23.8 \pm 5.6$. This significant correction indicates that $g^{(2)}(0)$ reported in Fig. 2 may contain a large contribution due to dark counts.

In summary, we have demonstrated a room temperature, telecommunications-band silicon heralded single photon source through spontaneous four-wave-mixing in a 35-ring silicon coupled resonator optical waveguide. Our work is a step towards highly functional quantum photonic chips that integrate single photon sources with waveguide quantum photonic circuits [6] and single photon counters [7] in a common silicon platform.

This work was supported by the National Science Foundation under grants ECCS-0642603, ECCS-0925399, NSF-GOALI collaboration with IBM, NSF-NIST supplement, and UCSD-Calit2. J. R. Ong acknowledges support from Agency for Science, Technology and Research (A*STAR) Singapore. We thank Nick Bertone from Optoelectronic Components for his help in setting up this collaboration. M.D. and I.A. acknowledge support under the Cooperative Research Agreement between the University of Maryland and NIST-CNST, Award 70NANB10H193.

-
- [1] J. L. O'Brien, A. Furusawa, and J. Vučković, *Nature Photonics* **3**, 687 (2009).
 - [2] A. Politi, M. J. Cryan, J. G. Rarity, S. Yu, and J. L. O'Brien, *Science* **320**, 646 (2008).
 - [3] J. C. F. Matthews, A. Politi, A. Stefanov, and J. L. O'Brien, *Nature Photonics* **3**, 346 (2009).
 - [4] L. Sansoni, F. Sciarrino, G. Vallone, P. Mataloni, A. Crespi, R. Ramponi, and R. Osellame, *Phys. Rev. Lett.* **105**, 200503 (2010).
 - [5] A. J. Shields, *Nature Photonics* **1**, 215 (2007).
 - [6] D. Bonneau, E. Engin, K. Ohira, N. Suzuki, H. Yoshida, N. Iizuka, M. Esaki, C. Natarajan, M. Tanner, R. Hadfield, S. Dorenbos, V. Zwiller, J. O'Brien, and M. Thompson, in *8th IEEE International Conference on Group IV Photonics (GFP)*, IEEE (IEEE, Piscataway, NJ, 2011) pp. 1–3.
 - [7] W. Pernice, C. Schuck, O. Minaeva, M. Li, G. Goltsman, A. Sergienko, and H. Tang, (2011), arXiv:1108.5299 [optics].
 - [8] H. J. Kimble, M. Dagenais, and L. Mandel, *Phys. Rev. Lett.* **39**, 691 (1977).
 - [9] P. Grangier, G. Roger, and A. Aspect, *Europhysics Letters* **1**, 173 (1986).
 - [10] C. K. Hong and L. Mandel, *Phys. Rev. Lett.* **56**, 58 (1986).
 - [11] S. Fasel, O. Alibart, S. Tanzilli, P. Baldi, A. Beveratos, N. Gisin, and H. Zbinden, *New J. Phys.* **6**, 163 (2004).

- [12] P. J. Mosley, J. S. Lundeen, B. J. Smith, P. Wasylczyk, A. B. U'Ren, C. Silberhorn, and I. A. Walmsley, *Phys. Rev. Lett.* **100**, 133601 (2008).
- [13] A. B. U'Ren, C. Silberhorn, K. Banaszek, and I. A. Walmsley, *Phys. Rev. Lett.* **93**, 093601 (2004).
- [14] O. Alibart, D. B. Ostrowsky, P. Baldi, and S. Tanzilli, *Opt. Lett.* **30**, 1539 (2005).
- [15] M. Lobino, G. D. Marshall, C. Xiong, A. S. Clark, D. Bonneau, C. M. Natarajan, M. G. Tanner, R. H. Hadfield, S. N. Dorenbos, T. Zijlstra, V. Zwiller, M. Marangoni, R. Ramponi, M. G. Thompson, B. J. Eggleton, and J. L. O'Brien, *Applied Physics Letters* **99**, 081110 (2011).
- [16] M. Fiorentino, P. L. Voss, J. E. Sharping, and P. Kumar, *IEEE Photonics Tech. Lett.* **14**, 983 (2002).
- [17] J. G. Rarity, J. Fulconis, J. Duligall, W. J. Wadsworth, and P. S. J. Russell, *Opt. Express* **13**, 534 (2005).
- [18] E. A. Goldschmidt, M. D. Eisaman, J. Fan, S. V. Polyakov, and A. Migdall, *Phys. Rev. A* **78**, 013844 (2008).
- [19] O. Cohen, J. S. Lundeen, B. J. Smith, G. Puentes, P. J. Mosley, and I. A. Walmsley, *Phys. Rev. Lett.* **102**, 123603 (2009).
- [20] J. E. Sharping, K. F. Lee, M. A. Foster, A. C. Turner, B. S. Schmidt, M. Lipson, A. L. Gaeta, and P. Kumar, *Optics Express* **14**, 12388 (2006).
- [21] K.-I. Harada, H. Takesue, H. Fukuda, T. Tsuchizawa, T. Watanabe, K. Yamada, Y. Tokura, and S.-I. Itabashi, *Opt. Express* **16**, 20368 (2008).
- [22] S. Clemmen, K. P. Huy, W. Bogaerts, R. G. Baets, P. Emplit, and S. Massar, *Opt. Express* **17**, 16558 (2009).
- [23] C. Xiong, C. Monat, A. S. Clark, C. Grillet, G. D. Marshall, M. J. Steel, J. Li, L. O'Faolain, T. F. Krauss, J. G. Rarity, and B. J. Eggleton, *Opt. Lett.* **36**, 3413 (2011).
- [24] A. B. Shehata, C. Scarcella, A. Tosi, and A. D. Frerar, *Proc. of IEEE, Ph.D. Research in Microelectronics and Electronics* **177**, 177 (2011).
- [25] K. F. Lee, J. Chen, C. Liang, X. Li, P. L. Voss, and P. Kumar, *Opt. Lett.* **31**, 1905 (2006).
- [26] J. Ong, M. Cooper, G. Gupta, W. Green, S. Assefa, F. Xia, and S. Mookherjea, *Opt. Lett.* **36**, 2964 (2011).
- [27] F. Morichetti, A. Canciamilla, C. Ferrari, A. Samarelli, M. Sorel, and A. Melloni, *Nature*

Communications **2** (2011).

- [28] M. Notomi, E. Kuramochi, and T. Tanabe, Nature Photonics **2**, 741 (2008).
- [29] Raw coincidences C_{raw} are counted over a 512 ps bin at zero time delay between the C–band and L–band paths. Raw accidentals (A_{raw}) are taken as the average over thirty separate 512 ps bins at time delays of $\{1\mu\text{s}, 2\mu\text{s}, \dots, 30\mu\text{s}\}$, corresponding to the 1 MHz trigger rate, with coincidences due to dark counts D determined in the same way. The uncertainties in A_{raw} and D are one standard deviation values and are propagated to generate the error bars in the CAR plot.
- [30] Coincidence and accidental rates at the CROW output are determined by taking the measured values and accounting for detector efficiency, filter losses, and output coupling loss from the CROW into the lensed fiber.
- [31] M. Beck, J. Opt. Soc. Am. B **24**, 2972 (2007).
- [32] N_{AB} and N_{AC} are given by the average detection rates on SPADS B and C multiplied by the integration time, respectively. N_A is the average photon detection rate on SPAD A multiplied by the integration time. The one standard deviation uncertainties on these values are propagated to generate the error bars in Fig. 3(a).